arXiv:1608.07599v1 [cond-mat.str-el] 26 Aug 2016

Bond patterns and charge order amplitude in $\frac{1}{4}$-filled charge-transfer solids

R.T. Clay,[1,*] A.B. Ward,[1] N. Gomes,[2] and S. Mazumdar[2,3]

[1] *Department of Physics and Astronomy and HPC² Center for Computational Sciences, Mississippi State University, Mississippi State MS 39762*

[2] *Department of Physics, University of Arizona Tucson, AZ 85721*

[3] *Department of Chemistry, University of Arizona Tucson, AZ 85721*

(Dated: August 30, 2016)

Metal-insulator transition accompanied by charge-ordering has been widely investigated in quasi-one-dimensional conductors, including in particular organic charge-transfer solids. Among such materials the $\frac{1}{4}$-filled band charge-transfer solids are of strong interest, because of the commensurate nature of the charge-ordering in these systems. The period-four charge-order pattern $\cdots 1100 \cdots$ here is accompanied by two distinct bond distortion patterns, giving rise to bond-charge-density waves (BCDW) of types 1 and 2. Using quantum Monte Carlo methods, we determine the phase diagram within the extended Hubbard Hamiltonian that gives both types 1 and 2 BCDW in the thermodynamic limit. We further investigate the effect of electron-electron and electron-phonon interactions on the amount of charge disproportionation. Our results show that between these two bond patterns, one (BCDW2) in general coexists with a large magnitude charge order, which is highly sensitive to electron-phonon interactions, while the other (BCDW1) is characterized by weak charge order. We discuss the relevance of our work to experiments on several $\frac{1}{4}$-filled conductors, focusing in particular on the materials $(EDO\text{-}TTF)_2X$ and $(DMEDO\text{-}TTF)_2X$ with large amplitude charge-order.

PACS numbers: 71.10.Fd, 71.45.Lr, 74.70.Kn

I. INTRODUCTION

Molecular charge transfer solids (CTS) are widely studied because of their many complex electronic states. Small structural changes can lead to very different electronic behaviors. These effects have been studied extensively in the quasi-one dimensional CTS, in particularly for the $\frac{3}{4}$-filled (with density $\rho = 0.5$ holes per molecule) materials $(TMTSF)_2X$ and $(TMTTF)_2X$, which become superconducting under the application of pressure.

The ground state of a one dimensional (1D) system of electrons with coupled lattice degrees of freedom is an insulating Peierls state. Quite generally at $\rho = 0.5$ the ground state is a bond-charge density wave (BCDW) with coexisting charge order (CO) and bond distortion and can be described by a Hamiltonian with electron-electron (e-e) and electron-phonon (e-p) interactions[1–3]. Experimentally, the properties of BCDWs in quasi-1D $\rho = 0.5$ CTS are observed to vary widely. In systems with type 1 BCDW, hereafter BCDW1, there occur *two* distinct transitions, a high temperature ($\approx$100 K) metal-insulator (MI) transition followed by a low temperature ($T \leq 20$ K) magnetic transition to a spin-gapped or antiferromagnetic state that coexists with CO with weak amplitude (we define the amplitude of the CO as the difference in charge densities between the charge-rich and charge-poor molecular sites.) The most well known examples of BCDW1 systems are in the $(TMTTF)_2X$ family. Systems with type 2 BCDW, hereafter BCDW2, are less widely known. There occurs a single MI transition in these systems which is accompanied by both a charge gap and a spin gap. Experimentally determined CO amplitudes in these cases are rather large[4]. One member of the BCDW2 family is $(EDO\text{-}TTF)_2PF_6$, where the MI transition temperature is 280 K and the CO amplitude is known to be approximately 0.9:0.1 [5–7]. The large CO amplitude has led to suggestions that interactions beyond e-e and e-p, such as molecular bending[8] or electronic polarization effects[9] are the driving forces behind the MI transition. Yet another system that belongs to this class is $(DMEDO\text{-}TTF)_2X$, X = ClO_4 and BF_4, where also there occurs a single MI transition that opens both a charge and spin gap simultaneously. It has been suggested that anion ordering drives the transition here[10]. The CO amplitude is currently unknown. One goal of our work is to show that both BCDW1 with small CO amplitude and BCDW2 with large CO amplitude can be understood within the same one-dimensional fundamental theoretical model, albeit within different parameter regions. The observed molecular bending[8] as well as cation-anion interactions[10] are consequences and not the

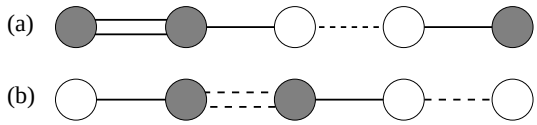

FIG. 1: Bond distortion patterns coexisting with $\cdots 1100 \cdots$ CO in the $\frac{1}{4}$-filled band. Filled (unfilled) circles indicate molecules with charge density $0.5 + \delta$ ($0.5 - \delta$). (a) BCDW2 with bond distortion pattern Strong-Medium-Weak-Medium (SMWM). Here the double line indicates a stronger bond (S) than a single line (M), and solid lines are stronger than dashed lines (W). (b) BCDW1 with pattern Strong-Weak-Strong-Weak′ (SWSW′). Here the single (S) bond is strongest, followed by double-dashed (W′) and single-dashed (W).

driving forces behind the *co-operative* transitions.

The bond distortion patterns corresponding to BCDW1 and BCDW2 are shown in Fig. 1. In both the charge density follows the pattern $\cdots 1100 \cdots$, where 1 (0) indicates a molecule with charge density $0.5+\delta$ ($0.5-\delta$). In BCDW2 (Fig. 1(a)) the strongest bond is between the two large charge densities (within the dimer), and the hopping integrals follow the pattern strong-medium-weak-medium (SMWM). In BCDW1 (Fig. 1(b)), the pattern of hopping integrals in the ground state is instead strong-weak-strong-weak′ (SWSW′) in Fig. 1(b)), where the W′ bond is slightly weaker than the W bond.

In this paper we perform a systematic numerical study of these two states, with a goal of fully determining the phase diagram as well as BCDW order parameters (amplitude of the CO and bond distortion) in the thermodynamic limit. We show that larger charge disproportionation coexists with BCDW2, with magnitudes that are consistent with experimental results. On the other hand, for BCDW1, we show that the CO amplitude is significantly smaller.

The outline of the paper is as follows: in Section II we define the model and theoretical quantities, followed by calculations for the phase diagram in II A, and BCDW order parameters in II B. In Section III we compare our results with experimental studies of several materials.

II. RESULTS

A well established minimal model for the 1D CTS is the 1D Peierls-extended Hubbard model,

$$\begin{aligned} H &= -\sum_{i\sigma}[t-\alpha\Delta_i](c^\dagger_{i+1,\sigma}c_{i,\sigma}+H.c.)+\frac{1}{2}K_1\sum_i\Delta_i^2 \\ &+ g\sum_i\nu_i n_i+\frac{1}{2}K_2\sum_i\nu_i^2 \\ &+ U\sum_i n_{i,\uparrow}n_{i,\downarrow}+V\sum_i n_{i+1}n_i. \end{aligned} \quad (1)$$

In Eq. 1, $c^\dagger_{i,\sigma}$ ($c_{i,\sigma}$) creates (annihilates) an electron of spin σ on site i, $n_{i,\sigma}$=$c^\dagger_{i,\sigma}c_{i,\sigma}$, and n_i=$n_{i,\uparrow}+n_{i,\downarrow}$. Δ_i is the deviation of the bond between sites i and $i+1$ from its equilibrium length and α is the inter-site e-p coupling with spring constant K_1. Intra-molecular distortions on each molecule are parameterized by the phonon coordinate ν_i; g is the intra-site e-p coupling with K_2 its corresponding spring constant. U and V are the onsite and nearest-neighbor Coulomb interactions respectively. We give energies in units of t.

At $\frac{1}{4}$-filling ($\rho = 0.5$), charge- and bond-ordering at $2k_F$ (period four) or $4k_F$ (period two) dominate. The occurrence of $4k_F$ CO requires $V > V_c$, where the critical value[11] $V_c = 2$ in the limit $U \to \infty$ but is larger than 2 for finite U (see Fig. 3). In applying Eq. 1 to the 1D CTS, it is also expected that $V < \frac{U}{2}$, based on comparison to $\rho =$ 1 1D CTS[12]. Here we restrict our analysis to regions of the phase diagram with $V < V_c$ and $V < \frac{U}{2}$. Throughout this region bond ordering is in general a mixture of period four and period two distortions. A general form for Δ_j can be written as[1]

$$\Delta_j = \Delta_0[a_2\cos(2k_F j-\phi_2)+a_4\cos(4k_F j-\phi_4)], \quad (2)$$

where Δ_0 is the overall amplitude of the bond distortion, a_2 and a_4 are the amplitude of $2k_F$ and $4k_F$ components respectively, and ϕ_2 and ϕ_4 their phases.

Exact diagonalization solutions of Eq. 1 have found several possible BCDW states[1,2]. In the region of phase space we consider two different BCDW solutions are found, shown schematically in Fig. 1(a) and (b) and labeled BCDW2 and BCDW1 below. Note that a second $2k_F$ charge pattern, $\cdots 2000 \cdots$ is also possible, but only in the limit of very weak e-e interactions[1]; we will not consider it here.

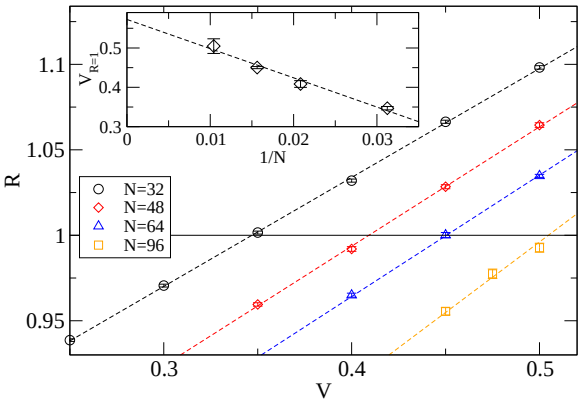

FIG. 2: (color online) (a) $R = \chi_B(4k_F)/\chi_B(2k_F)$ as a function of V with $U = 6.25$. Circles, diamonds, triangles, and squares are for 32, 48, 64, and 96 site chains, respectively. The inset shows the finite-size scaling of $V_{R=1}$, the V for which $R = 1$

.

A. Phase diagram

While several previous works have demonstrated the presence of BCDW2 and BCDW1 in small-lattice exact diagonalization calculations, the parameter regions of these two phases have not been mapped out in the thermodynamic limit. Here we determine the phase boundary between the BCDW2 and BCDW1 in the limit of 0^+ e-p coupling, i.e. the phase boundaries that occur unconditionally for a given U and V in the thermodynamic limit.

In Eq. 2 the phase angles for both BCDW states are[1] $\phi_2 = \frac{\pi}{2}$ and $\phi_4 = 0$. While BCDW2 is nearly a pure $2k_F$ bond distortion, BCDW1 requires a significant $4k_F$ component. The minimum a_4 in Eq. 2 for the BCDW1 pattern occurs when the 'S' and 'W′' bonds are of equal strength. From this one can derive the condition that $a_4/a_2 > \frac{1}{2}$ in the BCDW1 phase[1,13]. Further assuming

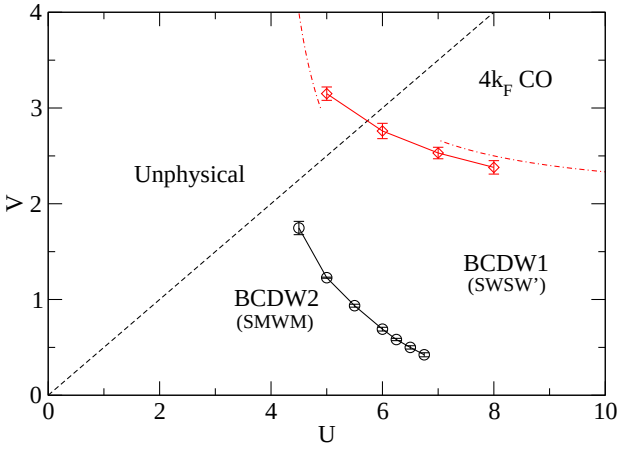

FIG. 3: (color online) Zero temperature phase diagram of Eq. 1 in the limit of 0^+ e-p interactions at $\frac{1}{4}$ filling. Open points are the boundary between BCDW2 and BCDW1 regions. Diamonds and dot-dashed lines mark the boundary to the $4k_F$ CO region (see Ref. 2). The dashed line indicates the region of physical relevance for organic CTS, $V \lesssim \frac{U}{2}$.

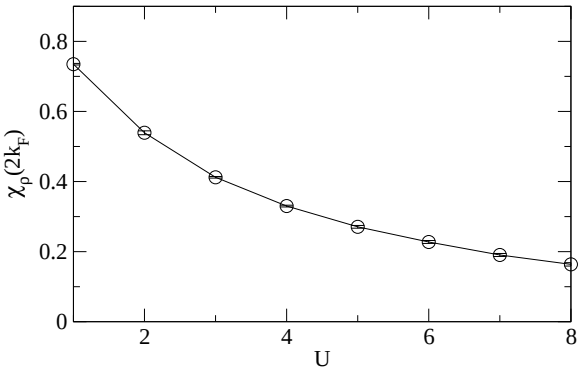

FIG. 4: $2k_F$ charge susceptibility as a function of U for a 48 site chain with $V = U/4$, $\alpha = g = 0$, and inverse temperature $\beta = 192$.

the normalization $a_2 + a_4 = 1$, this implies $a_4 > \frac{1}{3}$ for BCDW1.

The tendency to bond distortion at a wavevector q is measured by the bond susceptibility[14], $\chi_B(q)$, defined as

$$\chi_B(q) = \frac{1}{N}\sum_{j,l}\int_0^\beta e^{iq(j-l)}\langle \tilde{B}_j(\tau)\tilde{B}_l(0)\rangle d\tau. \qquad (3)$$

In Eq. 3, $\tilde{B}_j(\tau) = e^{-\tau H}\tilde{B}_j e^{\tau H}$ where $\tilde{B}_j = B_j - \langle B\rangle$ and $B_j = \frac{1}{2}\sum_\sigma (c^\dagger_{j+1,\sigma}c_{j,\sigma} + H.c.)$. β is the inverse temperature and N the number of sites. The BCDW2/BCDW1 phase boundary corresponds to a specific ratio of $4k_F$ to $2k_F$ bond distortion and may therefore in the limit of 0^+ e-p phonon coupling be determined by comparing $\chi_B(2k_F)$ and $\chi_B(4k_F)$. The discrete Fourier transform of $\Delta_j\Delta_l$ with respect to $(j-l)$ is $\Delta_0^2 a_2^2 N/4$ at $q = \pi/2$ and $\Delta_0^2 a_4^2 N$ at $q = \pi$. Therefore, in the limit of 0^+ e-p coupling $\chi_B(4k_F)/\chi_B(2k_F) = 4a_4^2/a_2^2$ and the BCDW1 phase will occur when $\chi_B(4k_F)/\chi_B(2k_F) > 1$. The bond distortion changes smoothly between the two phases without any discontinuity in the bond distortion or other observables.

We use the Stochastic Series Expansion (SSE) quantum Monte Carlo method with directed loop updates to calculate $\chi_B(q)$[15,16]. SSE is free from the Fermion sign problem in 1D and provides exact (within statistical errors) results at finite temperatures. We calculated the ratio $R = \chi_B(4k_F)/\chi_B(2k_F)$ for periodic systems of $N =$ 32, 48, 64, and 96 sites with an inverse temperature of $\beta = 4N$, which is a low enough temperature to give essentially ground state results. $\chi_B(4k_F)$ increases with increasing V; for each system size, the V where $R = 1$ was determined keeping U fixed, as shown in Fig. 2. We then performed a finite-size scaling using a linear fit of the transition points to $1/N$; a typical fit is shown in the inset of Fig. 2. Fig. 3 shows the complete phase diagram in the (U,V) plane. In Fig. 3 we also include the boundary for the $4k_F$ CO phase[11] from Reference 2, which are determined from the condition that the Luttinger Liquid exponent $K_\rho > \frac{1}{3}$, indicating dominant $4k_F$ charge fluctuations[17]. The dot-dashed lines in Fig. 3 are the result of second order perturbation theory about the $U \to \infty$ and $V \to \infty$ limits[11,18]. In the rest of the paper we focus on the regions of the phase diagram occupied by BCDW1 and BCDW2. The phase boundary between $4k_F$ CO and BCDW1 has been discussed extensively in our previous work[2,12].

B. Charge order amplitude

We define the amplitude of the CO as $\Delta n = \langle n_{\rm large}\rangle - \langle n_{\rm small}\rangle$, where $n_{\rm large}$ and $n_{\rm small}$ are the charge densities on the charge-rich and charge-poor molecules. Δn is of great experimental interest and can be measured optically[19] and by NMR[20]. Theoretically, Δn is difficult to predict from Eq. 1, as it depends on the precise values of the e-p coupling constants α and g which are difficult to estimate.

In the limit of $\alpha = g = 0$, the $2k_F$ charge susceptibility ($\chi_\rho(q)$) is defined as in Eq. 3 with $\tilde{B}_j$ replaced by $n_j - \langle n\rangle$) decreases with increasing U[21], implying that Δn is smaller in BCDW1 compared to BCDW2. In Fig. 4 we show $\chi_\rho(2k_F)$ as a function of U calculated along the line $V = U/4$ which crosses the BCDW2/BCDW1 boundary. Fig. 4 shows that differences in e-e correlation alone can account for approximately a factor of four in the magnitude of Δn between the most weakly-correlated CTS salts compared to those with strong e-e correlations, assuming equal e-p coupling strengths.

To calculate Δn in Eq. 1 with e-p interactions, we use a zero temperature variational quantum Monte Carlo using a matrix-product state basis (MPS-QMC)[4,22]. Matrix-product states are extremely efficient for representing the wavefunctions of interacting 1D quantum systems.

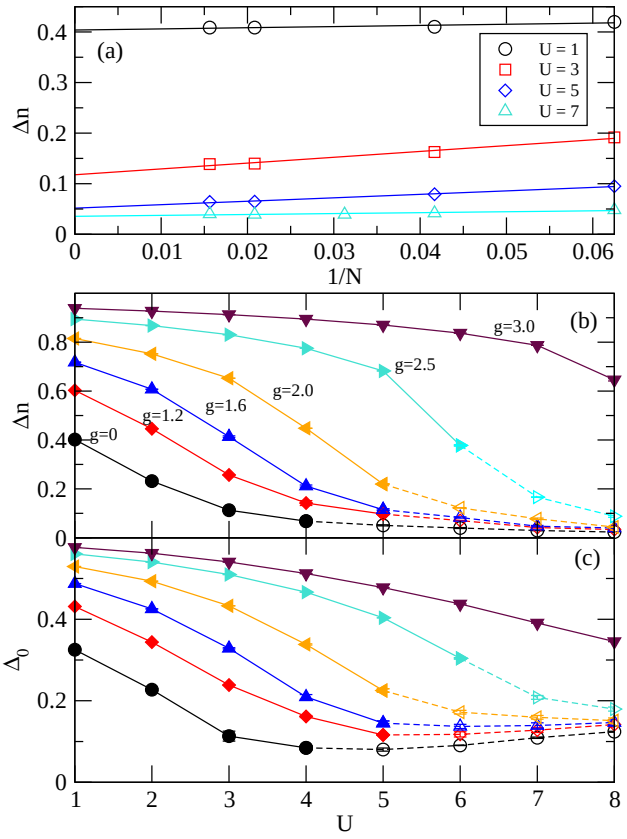

FIG. 5: (color online) Results of self-consistent MPS calculations (see text). For all panels $V = U/4$. (a) Finite size scaling of the charge order amplitude Δn versus inverse chain length with $\alpha = 1.2$ and $g = 0$. Lines are linear fits. (b) Finite-size scaled Δn as a function of U and g, with $\alpha = 1.2$. (c) The overall amplitude of the bond distortion (see Eq. 2) for the parameters of (b). In both (b) and (c) the filled (open) points correspond to BCDW2 (BCDW1) and lines are guides to the eye.

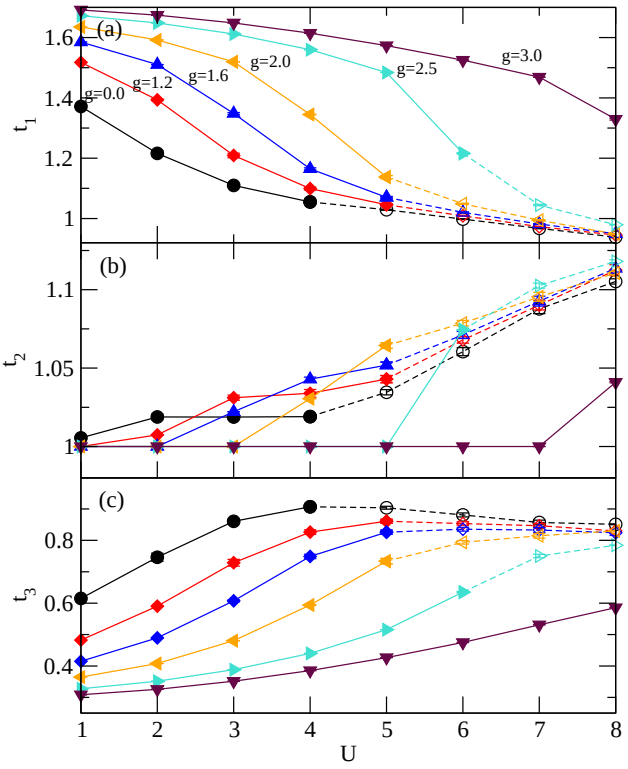

FIG. 6: (color online) Hopping integrals for the same parameters as Fig. 5.

The MPS-QMC method variationally optimizes the MPS matrices from random starting values using stochastic optimization[22]. One advantage of MPS-QMC is that periodic systems can be easily treated. Further details of the method are given in Reference 4. To handle the e-p degrees of freedom self-consistently, Δ_i in Eq. 1 is taken to be of the form of Eq. 2 with fixed ϕ_2 and ϕ_4. Fixing the bond distortion to this form is reasonable provided U and V are restricted to the BCDW2/BCDW1 region of the phase diagram—i.e. not too close to the $4k_F$ CO region. ν_i are taken with a constant magnitude ν and a fixed pattern $\cdots--++\cdots$ giving $\cdots 1100\cdots$ CO. Self-consistency equations for Δ_0, a_4, and ν are determined from[2]

$$\frac{\partial\langle H\rangle}{\partial\Delta_0} = 0 \qquad \frac{\partial\langle H\rangle}{\partial a_4} = 0 \qquad \frac{\partial\langle H\rangle}{\partial\nu} = 0.$$

For the results presented here, matrix dimensions D of up to 32 were used (see Reference 4). We used chain lengths from 16 up to 64 sites and finite-size scaled the results using linear extrapolation in $1/N$; Fig. 5(a) shows typical finite-size extrapolations for the case $\alpha = 1.2$ and $g = 0$.

The intra-site e-p interaction couples directly to the charge density and affects Δn strongly. We first choose a fixed α and vary g in Eq. 1. Figs. 5(b) and (c) summarize the results of these calculations. For $g \lesssim 2$, Δn versus U has a very similar functional shape as the $2k_F$ charge susceptibility in Fig. 4, confirming that e-e interactions strongly affect Δn. The maximum Δn for $g = 0$ is ≈ 0.4 at small U. As seen in Figs. 5(b) and (c), the bond pattern switches to BCDW1 at $U \approx 5$, which is consistent with the phase diagram in Fig. 3.

As shown in Fig. 5(b), in the BCDW2 phase, Δn is strongly enhanced by g up to nearly complete charge transfers of $\Delta n \approx 0.9$. BCDW1 however is characterized by small Δn for all g, which for most parameters choices is $\lesssim 0.1$. While in general weaker e-e correlations coincide with larger Δn, Fig. 5 shows that as g increases the phase boundary between BCDW2 and BCDW1 moves to larger U and V (i.e. the BCDW2/BCDW1 phase boundary in Fig. 3 moves towards the $4k_F$ CO phase with increasing g). Fig. 5 also shows that large enough g suppresses the BCDW1 phase altogether. It is also possible that large g in combination with U and V near the $4k_F$ CO phase results in $\cdots 1010\cdots$ CO[2].

Importantly, at large U, the strength of the bond distortion behaves differently from Δn. While the ampli-

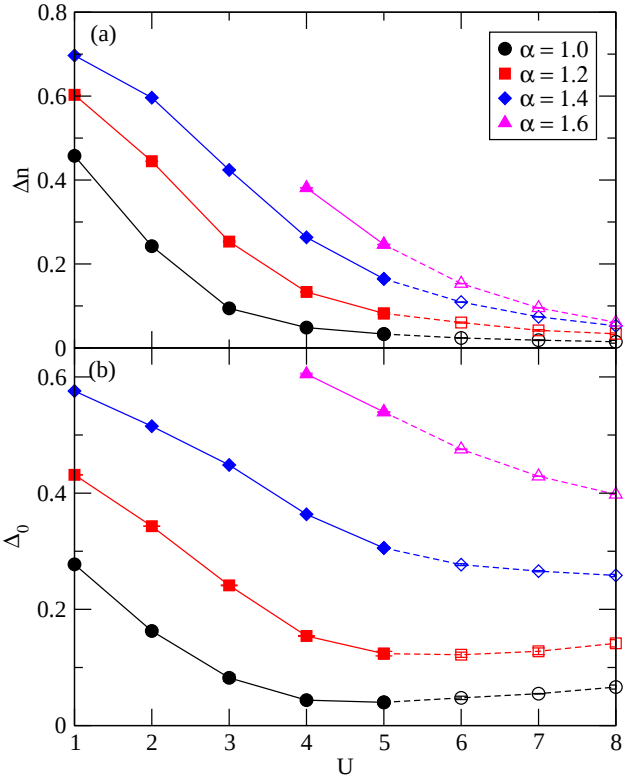

FIG. 7: (color online) (a) Finite-size scaled Δn as a function of U and α with $g = 1.2$. (c) The overall amplitude of the bond distortion (see Fig. 5(c)).

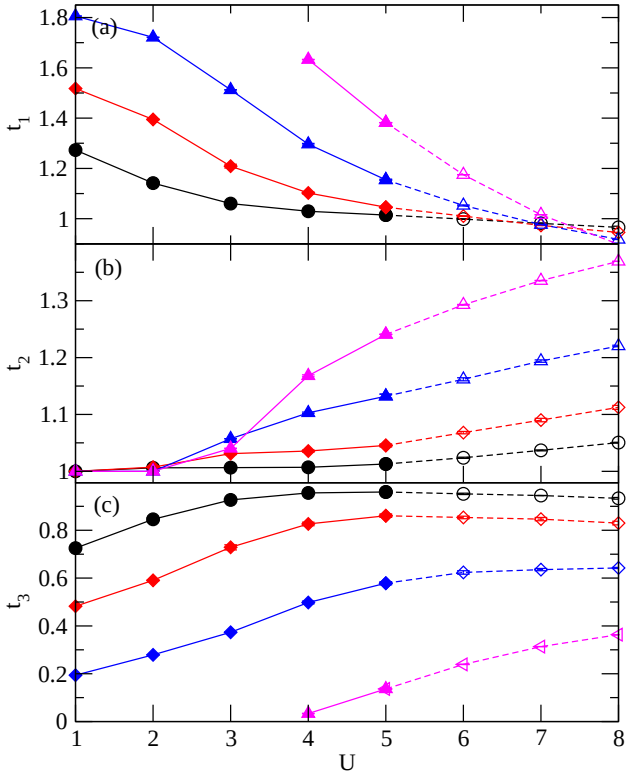

FIG. 8: (color online) Hopping integrals for the same parameters as Fig. 7.

tude of the $\cdots 1100 \cdots$ CO decreases continuously as the strength of e-e interactions increases, Fig. 5(c) shows that for weaker e-p interactions, the overall bond distortion strength Δ_0 first reaches a minimum at $U \approx 5$ and then *increases* again for larger U. The reason for this apparently counter-intuitive behavior is that while the $2k_F$ bond distortion decreases with increasing U, the $4k_F$ distortion increases with U (and V), causing the increase in Δ_0.

In the interest of comparing with experimental data, in Fig. 6 we show the actual hopping integrals. Corresponding to the charge order pattern $\cdots 1100 \cdots$ we define the '1−1' bond as t_1, the '1−0' and '0−1' bonds as t_2 and the '0−00' bond as t_3, respectively. In the BCDW2 pattern SMWM, t_1 is the strong S bond, t_2 the M bond, and t_3 the W bond. In the BCDW1 pattern SWSW′, t_1 is the W′ bond, t_2 the S bond, and t_3 the W bond. The decrease in t_1 in Fig. 6(a) and the simultaneous increase in t_2 in Fig. 6(b) are signatures of the crossover from BCDW2 to BCDW1 with increasing U.

In Fig. 7 we show the result of varying the inter-site e-p coupling α. Unlike g, α can only be varied over a relatively small range. For finite systems a minimum value of α is required for the lattice distortion to occur. For *too* large α the linear e-p coupling in Eq. 1 leads to a negative bond order for the weakest bonds indicating a failure of the linear coupling assumption (this occurs for $\alpha = 1.6$ and $U < 4$ in Fig. 7)[2]. Fig. 7 shows that varying α has a similar effect to varying g: stronger e-p coupling can enhance Δn strongly in the BCDW2 region, and at the same time moves the system towards the BCDW2 phase. Fig. 8 further shows the hopping integrals in this case. Increasing α can strongly increase the amplitude of the bond distortion in BCDW1 (see strong increase in Fig. 8(b)), however Δn remains small.

Summarizing our data, in the BCDW2 region Δn can have any value up to ≈ 0.9 depending on the e-e and e-p interaction strengths. However, regardless of the choice of e-e interactions and e-p coupling strength, Δn in the BCDW1 region is always small—the maximum in all of our calculations was $\Delta n \approx 0.2$. More typically Δn in the BCDW1 region is in the range $0.05 \sim 0.1$.

III. DISCUSSION

A. BCDW2

Below we discuss two families of CTS whose low-temperature insulating states show the BCDW2 bond pattern, $(EDO\text{-}TTF)_2X$ (X = PF_6 and AsF_6) and $(DMEDO\text{-}TTF)_2X$ (X = ClO_4 and BF_4). In each of these materials the MI transition has been attributed to different effects, such as e-p and coupled molecular bending[8] or electrical potential bias[9] in $(EDO\text{-}TTF)_2X$, and anion

ordering in $(DMEDO\text{-}TTF)_2X$[10]. We argue that these are instead *cooperative* effects, which are particularly obvious due to the large magnitude of Δn and bond distortion found in BCDW2. We expect that other 1D CTS with the BCDW2 distortion will show similarly strong effects at the MI transition. While these secondary effects will enhance the amplitude of the BCDW, they are not the principal driver of the transition, which is instead the underlying tendency to distortion of the quasi-1D electron system. The features common to BCDW2 are clearly seen by comparing $(EDO\text{-}TTF)_2X$ and $(DMEDO\text{-}TTF)_2X$, which show the same molecular stack distortion but quite different secondary effects.

$(EDO\text{-}TTF)_2X$: In $(EDO\text{-}TTF)_2X$ the MI transition is first order and occurs at 280 K and 268 K for X=PF_6 and AsF_6, respectively[5]. A third salt, X=ClO_4, has an even higher transition temperature, greater than 337 K[23]. In $(EDO\text{-}TTF)_2PF_6$ the experimentally estimated CO amplitude is rather large, with estimates of Δn from optical measurements of 0.92 (T=6 K)[6] or from X-ray measurements of 0.6 (T =260 K)[7]. Above the transition, the molecular overlaps along the EDO-TTF stacks are nearly uniform with only a slight dimerization[5]. Below the transition the overlap integrals follow the pattern SMWM[5].

Several observations indicate that intra-site e-p interactions are strongly involved in the MI transition. At the transition, the EDO-TTF molecules bend significantly[5], with the dihedral angles changing by more than 5°. The position of the anions also shift, with a periodic modulation that matches that of the EDO-TTF stacks[5]. Optical studies of $(EDO\text{-}TTF)_2X$ have suggested that the observed high sensitivity to photoexcitation is likely due to strong electron-lattice coupling[24].

$(DMEDO\text{-}TTF)_2X$: Here the MI transition is at 190 K and 210 K for X=ClO_4 and BF_4, respectively[10,25]. Above the MI transition the organic molecules are stacked uniformly, and like $(EDO\text{-}TTF)_2X$ the low temperature overlap integrals are in the SMWM pattern[10]. Simultaneously with the stack distortion, the anion positions shift, moving closer (further) towards molecules with large (smaller) hole density. The authors of Reference 10 ascribe the MI transition to anion ordering, as in $(TMTSF)_2ClO_4$. Note, however, that in contrast to $(TMTSF)_2ClO_4$ there is no simple rotational ordering of the ClO_4 anion in $(DMEDO\text{-}TTF)_2ClO_4$. Rather the Cl atom of the ClO_4 group moves towards and away from charge-rich and charge-poor molecules, which is a simple electrostatic effect. While Δn estimated from carbon-carbon bond lengths appears to be small (this method of estimating CO amplitude however has large errors)[10], we predict that optical measurements will find large Δn in this material.

To obtain the large Δn found in $(EDO\text{-}TTF)_2X$, our results of Section II show that large intra-site e-p coupling (and moderate or small e-e correlations) are required. The strong coupling to molecular bending in $(EDO\text{-}TTF)_2X$ shows that intra-molecular modes are coupled strongly in this case. Similarly, the large Δn will lead to large potential energy differences[9]. In both $(EDO\text{-}TTF)_2X$ and $(DMEDO\text{-}TTF)_2X$, electrostatic effects will shift the position of the anions.

B. BCDW1

As we have considered the thermodynamics of materials with the BCDW1 distortion in previous works[2,12], we will not discuss them in detail here. The BCDW1 state can be visualized as a second dimerization of a dimer lattice. In this case two thermodynamic transitions are expected, with the intermediate temperature state having either dimerization or $4k_F$ CO[2,12]. What the present calculations show is that in the ground state, the expected CO amplitude in BCDW1 is quite small and may be difficult to detect experimentally. This should also be taken into consideration in searches for CO in two dimensional CTS[26]. To detect the presence of BCDW1, it may be easier to focus on the pattern of bond distortion rather than the amount of CO.

Empirically, CTS showing the BCDW1 distortion are more likely to show superconductivity (SC) under pressure[4]. We have suggested that unconventional SC in $\rho = 0.5$ materials arises from the delocalization of the ('1−1') singlet pairs formed in the insulating Paired Electron Crystal (PEC), which has the same CO pattern $\cdots 1100 \cdots$ as BCDW1 and BCDW2[27–29]. Within such a model, the effective mass of the singlet is smaller in the BCDW1 because of the weaker binding, and hence the mobility of inter-dimer pairs here would be expected to be large, allowing a transition to a paired liquid state under the application of pressure[28]. On the other hand, the intra-dimer pairs with large Δn found in BCDW2 materials would tend to remain in an insulating state.

IV. ACKNOWLEDGMENTS

This work was supported by the Department of Energy grant DE-FG02-06ER46315. Part of the calculations were performed using resources of the National Energy Research Scientific Computing Center (NERSC), which is supported by the Office of Science of the U.S. Department of Energy under Contract No. DE-AC02-05CH11231.

* Electronic address: r.t.clay@msstate.edu

[1] K. C. Ung, S. Mazumdar, and D. Toussaint, Phys. Rev.

Lett. **73**, 2603 (1994).
[2] R. T. Clay, S. Mazumdar, and D. K. Campbell, Phys. Rev. B **67**, 115121 (2003).
[3] S. Mazumdar, R. T. Clay, and D. K. Campbell, Phys. Rev. B **62**, 13400 (2000).
[4] R. T. Clay, J. P. Song, S. Dayal, and S. Mazumdar, J. Phys. Soc. Jpn. **81**, 074707 (2012).
[5] A. Ota, H. Yamochi, and G. Saito, J. Mater. Chem. **12**, 2600 (2002).
[6] O. Drozdova, K. Yakushi, K. Yamamoto, A. Ota, H. Yamochi, G. Saito, H. Tashiro, and D. B. Tanner, Phys. Rev. B **70**, 075107 (2004).
[7] S. Aoyagi, K. Kato, A. Ota, H. Yamochi, G. Saito, H. Suematsu, M. Sakata, and M. Takata, Angew. Chem. Int. Ed. **43**, 3670 (2004).
[8] M. Tsuchiizu and Y. Suzumura, Phys. Rev. B **77**, 195128 (2008).
[9] K. Iwano and Y. Shimoi, Phys. Rev. B **77**, 075120 (2008).
[10] S. Kumeta, T. Kawamoto, T. Shirahata, Y. Misaki, and T. Mori, J. Phys. Soc. Jpn. **85**, 094701 (2016).
[11] F. Mila and X. Zotos, Europhys. Lett. **24**, 133 (1993).
[12] R. T. Clay, R. P. Hardikar, and S. Mazumdar, Phys. Rev. B **76**, 205118 (2007).
[13] In References 1 and 4 the bond distortion pattern is written in terms of u_j, the displacement of the jth site from equilibrium, with $2k_F$ and $4k_F$ weights r_2 and r_4. In the present notation $\Delta_j = u_{j+1} - u_j$. The ratio of $4k_F$ to $2k_F$ components required for the BCDW1 phase was quoted incorrectly in these references–rather than 0.41, $r_4/r_2 > \frac{\sqrt{2}}{4+\sqrt{2}} = 0.26$ for the BCDW1 pattern.
[14] J. E. Hirsch and D. J. Scalapino, Phys. Rev. B **29**, 5554 (1984).
[15] A. W. Sandvik, J. Phys. A **25**, 3667 (1992).
[16] O. F. Syljuasen and A. W. Sandvik, Phys. Rev. E **66**, 046701 (2002).
[17] J. Voit, Rep. Prog. Phys. **58**, 977 (1995).
[18] H. Q. Lin, D. K. Campbell, and R. T. Clay, Chinese J. Phys. **11**, 1 (2000).
[19] M. Dressel, M. Dumm, T. Knoblauch, and M. Masino, Crystals **2**, 528 (2012).
[20] F. Zamborszky, W. Yu, W. Raas, S. E. Brown, B. Alavi, C. A. Merlic, and A. Baur, Phys. Rev. B **66**, 081103 (2002).
[21] J. E. Hirsch and D. J. Scalapino, Phys. Rev. B **27**, 7169 (1983).
[22] A. W. Sandvik, Phys. Rev. Lett. **101**, 140603 (2008).
[23] A. Ota, H. Yamochi, and G. Saito, Synth. Metals **133-134**, 463 (2003).
[24] M. Chollet, L. Guerin, N. Uchida, S. Fukaya, H. Shimoda, T. Ishikawa, K. Matsuda, T. Hasegawa, A. Ota, H. Yamochi, et al., Science **307**, 86 (2005).
[25] J. M. Fabre, S. Chakroune, A. Javidan, L. Zanik, L. Ouahab, S. Golhen, and P. Delhaes, Synth. Metals **70**, 1127 (1995).
[26] K. Sedlmeier, S. Elsässer, D. Neubauer, R. Beyer, D. Wu, T. Ivek, S. Tomic, J. A. Schlueter, and M. Dressel, Phys. Rev. B **86**, 245103 (2012).
[27] S. Mazumdar and R. T. Clay, Int. J. Quant. Chem. **2014**, 1053 (2014).
[28] N. Gomes, W. W. De Silva, T. Dutta, R. T. Clay, and S. Mazumdar, Phys. Rev. B **93**, 165110 (2016).
[29] W. W. De Silva, N. Gomes, S. Mazumdar, and R. T. Clay, Phys. Rev. B **93**, 205111 (2016).